Dynamic Nuclear Polarization with Conductive Polymers

Quentin Stern,*[a] Guillaume Verhaeghe,[a] Théo El Daraï,[a,b] Damien Montarnal,[b] Nghia Huu Le,[b] Laurent Veyre,[b] Chloé Thieuleux,[b] Charlotte Bocquelet,[a] Olivier Cala,[a] Sami Jannin[a]

[a] Dr. Q. Stern, G. Verhaeghe, Dr. T. El Daraï, C. Bocquelet, Dr. O. Cala, Pr. S. Jannin
Université Claude Bernard Lyon 1, CRMN UMR-5082, CNRS, ENS Lyon
Villeurbanne 69100, France
E-mail: quentin.stern@protonmail.com

[b] Dr. D. Montarnal, Dr. N. Huu Le, Dr. L. Veyre, Dr. C. Thieuleux
Université de Lyon, Institut de Chimie de Lyon, Laboratory of Catalysis, Polymerization, Processes and Materials, CP2M UMR 5128 CNRS-UCB Lyon 1
CPE Lyon 43 Bd du 11 Novembre 1918, 69616 Villeurbanne, France

Abstract: The low sensitivity of liquid-state nuclear magnetic resonance (NMR) can be overcome by hyperpolarizing nuclear spins by dissolution dynamic nuclear polarization (dDNP). It consists of transferring the near-unity polarization of unpaired electron spins of stable radicals to the nuclear spins of interest at liquid helium temperatures, below 2 K, before melting the sample in view of hyperpolarized liquid-state magnetic resonance experiments. Reaching such a temperature is challenging and requires complex instrumentation, which impedes the deployment of dDNP. Here, we propose organic conductive polymers such as polyaniline (PANI) as a new class of polarizing matrices and report 1H polarizations of up to 5%. We also show that 13C spins of a host solution impregnated in porous conductive polymers can be hyperpolarized by relayed DNP. Such conductive polymers can be synthesized as chiral and display current induced spin selectivity leading to electron spin hyperpolarization close to unity without the need for low temperatures nor high magnetic fields. Our results show the feasibility of solid-state DNP in conductive polymers that are known to exhibit chirality-induced spin selectivity.

Keywords: nuclear magnetic resonance • dynamic nuclear polarization • spin hyperpolarization • conductive polymer

Table of contents

Dynamic nuclear polarization of polyaniline polymers

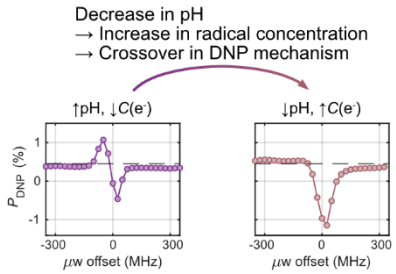

Introduction

The intrinsic low sensitivity of liquid-state nuclear magnetic resonance (NMR) and magnetic resonance imaging (MRI) can be overcome by hyperpolarizing nuclear spins[1] using dissolution dynamic nuclear polarization (dDNP).[2–5] dDNP is a three-step process where the sample is first hyperpolarized in the solid state at low temperatures (typically 1–2 K) and moderate magnetic fields (typically 3–7 T) by transferring the high polarization of unpaired electron spins to nuclear spins *via* microwave irradiation (μw); once the nuclear spins are hyperpolarized, the sample is dissolved in a superheated solvent and transferred to a liquid-state NMR spectrometer or MRI scanner, where the hyperpolarized solution-state NMR signals are detected. This approach to nuclear spin hyperpolarization is versatile and powerful, allowing one to polarize a broad range of molecules. It has led to a number of high-profile applications from medical imaging to spectroscopy.[3,4] However, unlike parahydrogen-induced polarization (PHIP) or spin-exchange optical pumping (SEOP), dDNP requires complex instrumentation and the use of liquid helium to reach low temperatures.[1] One of the main reasons behind this is that dDNP relies on the temperature T and magnetic field strength B_0 to establish high electron spin polarization at Boltzmann equilibrium

$$P_{\mathrm{eq}} = \tanh\left(\frac{\hbar\gamma B_0}{2k_{\mathrm{B}}T}\right), \qquad \text{Eq. 1}$$

where, $\hbar$, γ, and k_{B} are Planck's constant, the gyromagnetic ratio of the electron spin (in rad.s^{-1}), and Boltzmann's constant, respectively. Indeed, at 7.05 T and 1.6 K, the polarization of an electron spin in organic radicals like TEMPOL or trityl (with $g \approx 2$) is $P_{\mathrm{eq}} \approx 99.47\%$, allowing one to achieve nuclear polarization approaching unity. An alternative approach to using low temperatures to reach high electron spin polarization is to perform DNP from hyperpolarized electrons. DNP from color centers in diamonds[6] and photoexcited triplet states[7,8] has been proposed to this end. Although these methods can reach high nuclear polarization in the polarizing media itself, transferring the accrued polarization to molecules of interest remains challenging for several reasons. In particular, each electron hyperpolarization event, ideally followed by a transfer to a nuclear spin, is mediated by the absorption of a visible light photon. This involves substantial energy (typically several millijoules) and needs to be repeated at high rates (typically several kilohertz) to generate significant bulk nuclear magnetization per unit of time. Then, the magnetization needs to be further transferred to the molecules of interest across the polarizing media interface, which is another challenge yet to be tackled.

When Overhauser first introduced the concept of DNP in 1953,[9] he proposed to use conductive electrons in metals. The phenomenon was then observed experimentally by Carver and Slichter the same year on ^{7}Li in bulk Li.[10] We propose here a return to the origins of DNP with conduction electrons but in conductive organic polymers rather than in metals.[11,12] Such conductive polymer matrices can be used as versatile polarizing agents. Chiral conductive polymers are promising because electron spins can be hyperpolarized close to unity simply by flowing an electric current through the polymer, an established phenomenon routinely used in spintronics known as chirality-induced spin selectivity (CISS).[13–16] One could perform efficient DNP without relying on low temperatures, high fields, or high-power pulsed lasers, but rather using electron spins hyperpolarized by electrical power in a chiral conductive polymer. In 2022, Milani *et al.* reported heterogeneous Overhauser DNP on polyaniline (PANI) to polarize ^{1}H spins in water at room temperature.[17] PANI is a readily-available polymer that has been abundantly studied and for which CISS has been reported.[18] Because PANI polymers can be made porous,[19] they can be used to polarize arbitrary solutions by cross-polarization DNP (CP-DNP) as shown below.[20,21]

Here, we present the first results of solid-state DNP on and with PANI. A possible future goal would be to work at higher temperatures (typically in liquid nitrogen, i.e., at 77 K) and lower fields (typically 0.3–1 T) with electron hyperpolarization generated by CISS. We establish a first milestone in this direction by demonstrating DNP with thermally polarized electrons using our current DNP polarizer, which operates at 7.05 T between 1.6 and 4.3 K. Starting from commercially available PANI products, modified PANI samples were prepared with controlled electron spin concentration by partially protonating the imine functional group in an acidic aqueous solution and subsequently lyophilizing the powder. The concentration of radicals as a function of the protonation level was quantified by continuous wave (CW) electron paramagnetic resonance (EPR) at X-band and room temperature. For each PANI sample, a DNP profile (i.e., a plot of the polarization under DNP as a function of the μw irradiation frequency) was measured at 1.6 K and 7.05 T. These measurements revealed a surprising complexity of DNP mechanisms, with a crossover from a dispersive pattern at low radical concentration to a negative absorptive pattern at higher radical concentration. By analyzing the time evolution of saturation recovery curves at thermal equilibrium as a function of temperature, we found evidence that the mobility of the electron spins contributes to DNP and relaxation, and does not vary significantly between 1.6 and 4.3 K. Absolute ^{1}H polarizations of up to 5% were obtained (corresponding to a signal enhancement of $\varepsilon \approx 2'000$ compared to conventional NMR at 7.05 T and room temperature). Finally, we show that cross-reticulated porous PANI polymers can be impregnated with solutions to be polarized, here containing ^{13}C-labeled molecules. These solutions can be ^{13}C-hyperpolarized indirectly by ^{1}H-DNP followed by ^{1}H→^{13}C polarization transfer by CP. This paves the way to using PANI for hyperpolarization in a broad range of applications from complex mixture analysis and metabolomics to *in-vivo* metabolic imaging.

Results and Discussion

Tuning Electron Concentration in PANI

Figure 1A-B shows the structure of two forms of PANI, the emeraldine base (EB) and emeraldine salt (ES), respectively. The repeating unit of PANI-EB contains no unpaired electrons, while that of PANI-ES contains two unpaired electrons, in the form of positively charged spin ½ polarons. The fraction χ of ES units in the polymer therefore determines the radical concentration in the sample and can be controlled by partially protonating PANI-EB.[22] Protons and subsequent spin-

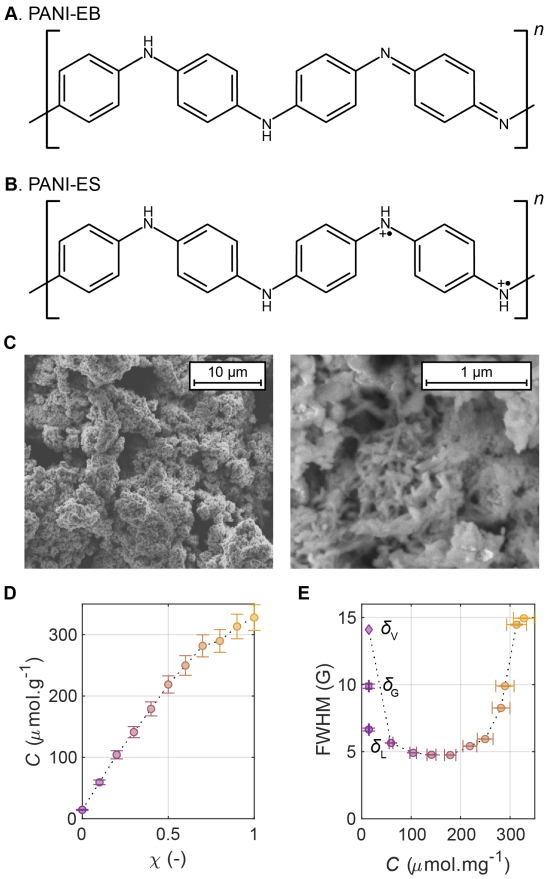

Figure 1: **A-B.** Structure of the repeating unit of PANI-EB and PANI-ES, respectively. **C.** SEM images of PANI-EB. **D.** Radical concentration in PANI measured by X-band CW-EPR at room temperature as a function of the protonation level χ. **E.** EPR signal FWHM as a function of the radical concentration, obtained by Voigt (for $\chi = 0$) and Lorentzian fitting (for $\chi > 0$) of the EPR signal integral. δ_G, δ_L, and δ_V are Gaussian, Lorentzian, and total Voigt broadenings, respectively (indicated by square, circles, and diamonds). The dashed black line follows the total broadening. The color code in panels D and E (gradient from purple to yellow at increasing radical concentration) is followed throughout the paper.

bearing quasiparticles do not distribute homogeneously in PANI. They preferentially aggregate in highly doped crystalline islands with size on the order of 5 nm, exhibiting high electron mobility (and hence high conductivity). These islands are surrounded by non-conductive disordered regions that contain fewer spins that exhibit lower mobility.[23–26] Electrons spins in the metal-like islands are exchange-coupled and give rise to Pauli susceptibility, while those in isolating regions are weakly interacting and give rise to Curie susceptibility.[22,23]

Based on a protocol from Ref. [27], eleven dry samples of PANI were prepared with χ from 0 to 1, that is, at various levels of conversion from PANI-EB to PANI-ES. Commercial PANI-EB polymers with a molecular weight of ≈ 50 kDa were purchased from Sigma-Aldrich. A scanning electron microscopy (SEM) image of the raw material is shown Fig. 1C, featuring domains in the sub-micrometer range. The radical concentration determined by X-band CW-EPR at room temperature is shown in Fig. 1D. The measured radical concentration for $\chi = 1$ is 328 ± 21 µmol.mg^{-1} (the error on the measured concentration only contains the contribution from the error on the calibration curve of the EPR signal intensity vs. radical concentration, see the Supplementary Material for more details). The measured radical concentration is a factor ~9 lower than the expected stoichiometric value, assuming that each chlorine anion is solvated by six water molecules. A possible explanation is that a fraction of the electron spins reorganizes as spinless doubly-charged bipolarons.[22,28] With $\chi = 0$, one would expect a radical concentration approaching 0. A non-negligible concentration of 14.4 ± 0.9 µmol.mg^{-1} was measured. Similar findings were reported and the EPR signal was attributed to Curie spins, i.e., spins located in disordered non-conductive regions.[29]

The EPR signal integrals were fitted with a Voigt profile, i.e., the convolution of Lorentzian and Gaussian lineshapes (see the Supplementary Material for details). Fig. 1E shows the fitted broadening parameters as a function of the measured radical concentration. The Lorentzian and Gaussian broadenings are indicated by δ_L and δ_G, respectively. The Gaussian contribution is found to be non-zero only for $\chi = 0$. In this case, the full width at half maximum (FWHM) obtained by the convolution of the Gaussian and Lorentzian broadenings, i.e., the width of the Voigt profile, is indicated by δ_V. For $\chi > 0$, because $\delta_G = 0$, the FWHM corresponds to δ_L. The Lorentzian width decreases as radical concentration increases up to about 200 µmol.mg^{-1} and increases rapidly as the concentration further increases. This is consistent with early reports on X-band EPR of PANI.[27,30] Indeed, it was shown that the EPR linewidth of PANI samples is dominated by homogenous broadening, i.e., spin-spin relaxation T_{2e}. As protonation increases, the mobility of the electron spin increases, which decreases the spectral density of the electron motion at the relevant frequencies and, in turn, increases T_{2e}. At higher protonation level, T_{2e} becomes limited by the electron spin-lattice relaxation time T_{1e} (extreme narrowing limit). In the presence of molecular oxygen (as is the case here), T_{1e} and T_{2e} decrease when protonation increases due to interaction with oxygen,[30] resulting in the dramatic observed increase in linewidth above 200 µmol.mg^{-1}. The large Gaussian broadening of $\delta_G = 9.9 \pm 0.2$ G observed for the lowest radical concentration is absent for all other radical concentrations. This is consistent with a signal dominated by Curie spins, which have lower mobility than the Pauli spins.[29]

It is worth noting that the EPR signal of PANI is asymmetric and so a free phase parameter had to be introduced in the Voigt and Lorentzian fits. Despite some outliers, the phase deviation increases from ~6° to ~10° from PANI-EB to PANI-ES (see Figures S2 and S3). This is due to the increase in the size of metal-like domains in PANI with protonation level.[31] As the domain size increase, they become comparable to the skin depth of the microwave field, leading to a Dyson-like lineshape.

For each sample, approx. 30 mg of the dry powder was placed in a KelF sample cup and immersed in the liquid helium bath of the DNP polarizer. A ^{1}H thermal equilibrium was first recorded at 1.6 K to quantify the nuclear polarization in the subsequent DNP experiments. A DNP profile, i.e., a series of

DNP build-ups as a function of the μw irradiation frequency was then recorded at 1.6 K. Figure 2a shows the DNP profiles for samples with χ values from 0 to 0.7, expressed as the maximum recorded polarization (i.e., the polarization for the last recorded spectrum of each build-up) P_{DNP}. The offset frequency of 0 corresponds to 197.630 GHz in the laboratory frame. The DNP profiles for χ between 0.8 and 1 do not show significant enhancement and thus are not shown. The sample with 105 μmol.mg^{-1} of radical yields the best DNP performance with maximum absolute polarization of 2.8% (see Fig. 2b). A crossover from a dispersive pattern at weak electron concentrations to a negative absorptive pattern at high electron concentrations dominates the DNP profiles. The dispersive pattern observed at the lowest radical concentration has been reported in a number of studies[32–37] (*vide infra*). In addition, most DNP profiles feature weak transitions that are likely due to the solid effect (SE) (most prominently for χ = 0.2 and 0.3).

Experimental Evidence of Electron Mobility

A peculiarity of PANI samples is that they provide conditions where both thermal mixing (TM) or the cross effect (CE), as well as the Overhauser effect (OE), can be expected. Indeed, high electron concentrations ensure sufficient electron-electron interactions for efficient electron-electron-nucleus triple-spin flips, and hence plausible TM/CE.[38] At the same time, the propensity of electrons to delocalize in PANI and the conductivity of PANI provide the conditions for the OE.[9,10] The mobility of the electron spins can be experimentally evidenced by the relaxation properties of ^{1}H spins in PANI.[24,39] At liquid helium temperatures, where nuclear self-relaxation is prohibitively slow, nuclear thermal relaxation is often dominated by electron-nuclear interactions, which is fundamentally the same process as DNP by TM, the CE, or the OE, except towards Boltzmann equilibrium.

Figure 3A shows thermal equilibrium saturation recovery experiments at 19 temperatures between 1.60 and 4.32 K (without μw irradiation) for the sample with χ = 0.2 (C = 105 ± 7 μmol.mg^{-1}). The signal intensity as a function of time $I(t)$ of each curve was fitted with a stretched exponential function

$$I(t) = I_\infty\left(1 - \exp\left(-\left(\frac{t}{T_1}\right)^\beta\right)\right), \qquad \text{Eq. 2}$$

where T_1 and β are the relaxation time constant and the stretched parameter (between 0 and 1), respectively. The average relaxation time constants $T_{1,av}$ were obtained from the fitted values of T_1 and β using

$$T_{1,av} = \frac{T_1}{\beta}\Gamma\left(\frac{1}{\beta}\right), \qquad \text{Eq. 3}$$

where Γ is the gamma function. The stretch factor was found to depend on temperature, varying linearly from 0.802 ± 0.003 to 0.51 ± 0.02 at 1.60 and 4.32 K, respectively (see Figure S5).

In insulating solids commonly used for DNP at liquid helium temperatures, relaxation is usually dominated by triple-spin flips of a nucleus with a pair of electron spins. The rate of this mechanism is known to be proportional to 1 – P_e^2, where P_e is the polarization of electron spins.[40] The origin of this factor is that triple-spin flips can only occur if the pair of electron spins is antiparallel, which has a probability of (1 – P_e^2)/4. In PANI, electron mobility brings other contributions to relaxation that are usually not encountered in dDNP experiments.[41] We attempted to fit the measured relaxation rates with the function

$$\frac{1}{T_{1,av}} = a(1 - P_e^2) + b, \qquad \text{Eq. 4}$$

where a and b are two constants and the Boltzmann electron polarization P_e is given by Eq. 1. An excellent agreement was

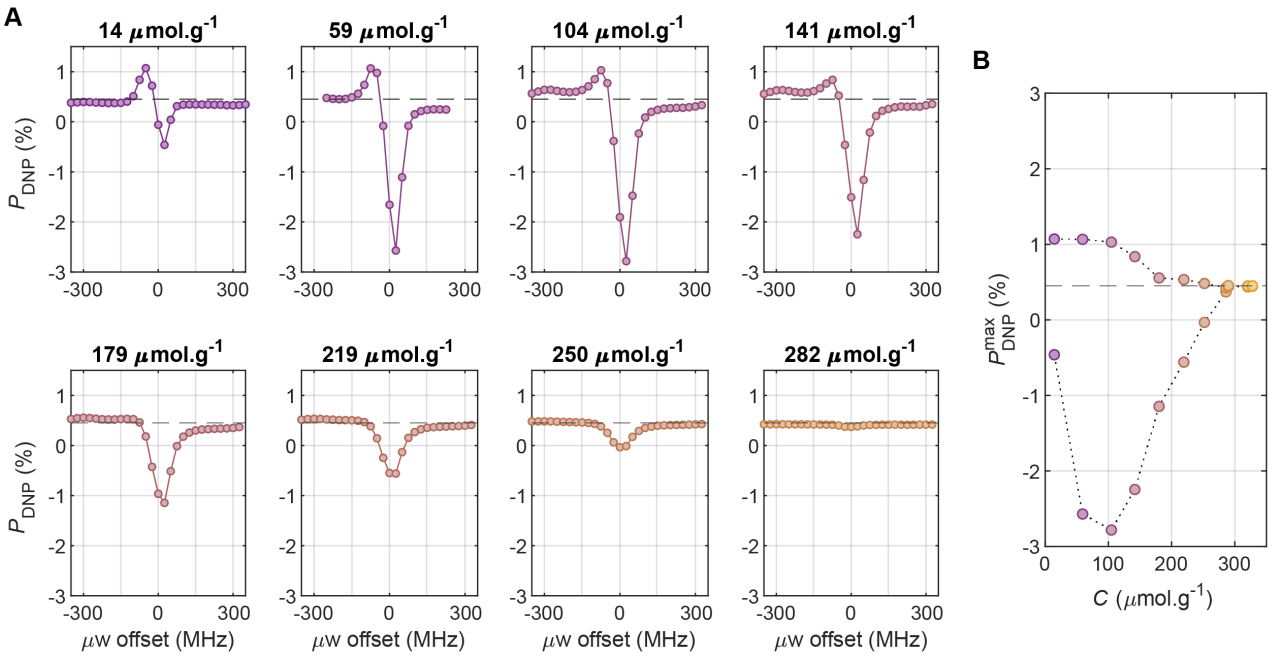

Figure 2: **A.** DNP profiles for PANI-EB protonated to level χ between 0 and 0.7 (the corresponding electron spin concentration is indicated on the plots), recorded using 1° pulses at 1.6 K and 7.05 T. The 0 of the μw frequency offset corresponds to 197.630 GHz in the laboratory frame. **B.** Final ^{1}H polarizations at the optimal μw frequencies for positive and negative DNP as a function of the radical concentration.

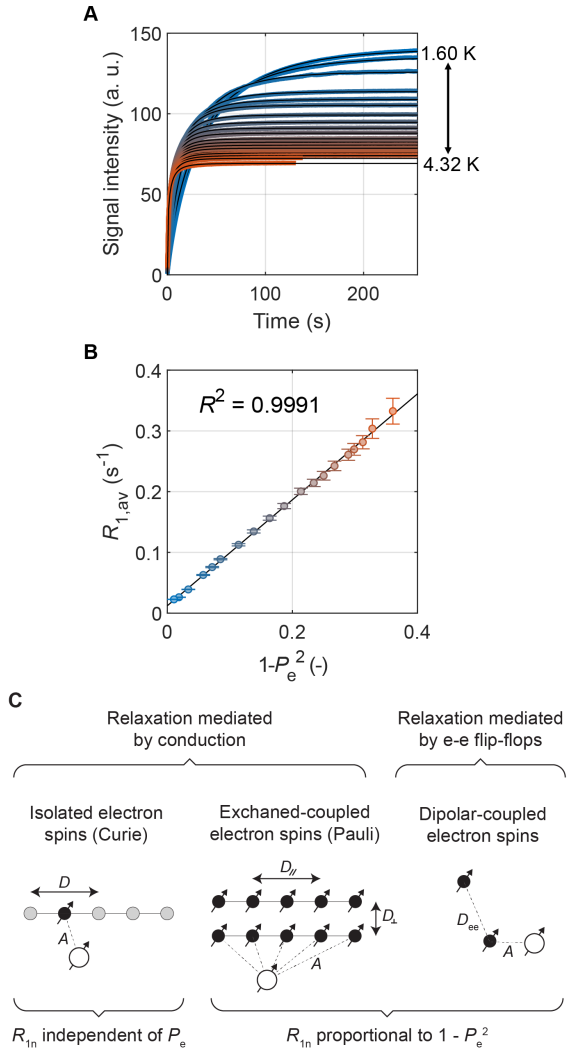

Figure 3: A. ^{1}H saturation recovery of PANI with χ = 0.2 (C = 105 ± 7 µmol.mg^{-1}) at various temperatures monitored with 1° pulses fitted with a stretched exponential function (see Eq. 2) (colored and black lines, respectively). **B.** Relaxation rate obtained in panel A plotted against 1 – P_e^2, where P_e is the electron polarization, fitted with Eq. 4 (colored dots and black line, respectively). **C.** Representation of electron spin configurations leading to different a P_e-dependent or independent nuclear relaxation. Black and white circles represent electron and nuclear spins, respectively. Grey circles represent positions where an isolated electron can delocalize. Dee and A are the electron-electron dipolar interactions and the electron nuclear hyperfine interactions, respectively.

found between the model and the experimental data for a = 0.87 ± 0.01 s^{-1} and b = 0.012 ± 0.003 s^{-1} (see black line in Fig. 3B), which shows that the dependence of a and b on temperature is very small, if any. The rate b bounds T_1(^{1}H) to a very low maximum value of ≈ 80 s. As a comparison, T_1(^{1}H) in DNP juice (i.e., an insulating solid) exceeds hours or tens of hours when the electron polarization approaches unity.[42] This result shows that electron mobility has a strong influence on relaxation and possibly on DNP for PANI at low temperatures.

We now discuss the possible origin of the P_e-dependent and -independent relaxation rates a and b. As mentioned previously, electrons in PANI are known to distribute heterogeneously, with fully protonated metal-like islands separated by non-protonated insolating regions. Nuclear relaxation in PANI is the result of the random motion or diffusion of Pauli spins among the doped islands.[22,43–45] To our knowledge, no studies on relaxation in conductive polymers, whether EPR on NMR, were performed in conditions where the polarization of the electron approaches unity, i.e., 1 – P_e^2 < 1. Therefore, the established relaxation model does not account for this factor.[22,43–45] Fig. 3C gives a visual representation of Pauli spins in a chain. As all positions that electron spins can occupy are full, the motion of fully polarized electrons gives rise to no net change in magnetization and should not induce any relaxation. Pauli spins should therefore contribute to the P_e-dependent nuclear relaxation coefficient a. In addition to Pauli susceptibility, PANI samples also exhibit Curie susceptibility, i.e., susceptibility from isolated (or at least weakly interacting) electron spins. These spins are usually trapped and do not contribute to the macroscopic conductivity of PANI polymers.[29] However, they are still part of a conjugated network and should have some level of local motion, similar to what is found in BDPA for example.[46,47] Random motion of an isolated spin will cause fluctuations of the magnetic field experienced by the nuclear spins regardless of the electron spin polarization. Curie spins are therefore likely to contribute to the nuclear relaxation coefficient b. It is not surprising that this mechanism is not mentioned in the literature on PANI polymers as it is about a/b ≈ 70 times weaker than relaxation by Pauli spins when the electron spin polarization is small, according to our measurements. Finally, we note that, relaxation *via* triple-spin flips is proportional to 1 – P_e^2 so this mechanism, if significant, would contribute to a.

The fact that coefficient a does not depend on temperature has implication for conduction in PANI. In conductive polymers, nuclear spins relax due to the random motion of electron spins along polymer chains (1D model) and from chain to chain (deviation from 1D, or quasi-1D model), described by diffusion coefficients $D_\parallel$ and $D_\perp$, respectively.[22,43–45] These two processes have different temperature dependences but were shown to reach a plateau below 50 K, for undoped PANI-EB and PANI-ES, in relaxometry studies using muon spin relaxation[48] and EPR[49], respectively. These studies were performed at temperatures down to 4 K. At high magnetic field, as is the case here, the spectral density responsible for nuclear spin-lattice relaxation is in the 1D limit, meaning that it is dominated by $D_\parallel$ with a minor contribution of $D_\perp$ (see Figure S9). The temperature-independence of a confirms the temperature independence of at least $D_\parallel$ between 1.6 and 4.3 K.

The homogeneous broadening of ^{1}H spins was found to increase from δ_L = 34.1 ± 0.2 s^{-1} to 36.7 ± 0.2 s^{-1} between 4.32 and 1.60 K by fitting the ^{1}H line with a Voigt profile (see Figures S6 and S7), while the inhomogeneous broadening remains constant (with δ_G = 27.6 ± 0.2 s^{-1} on average). The nuclear homogeneous broadening is proportional to the nuclear spin-spin decoherence rate R_2. Because it decreases when temperature increases, electron-electron interactions are probably not the dominating mechanism to nuclear decoherence. This broadening at decreasing temperature could be the result of decreasing mobility of the polymer chain,

as it is known that aromatic rings in PANI have torsional degrees of freedom.[28]

Polarizing Arbitrary Solutions in Porous PANI

CP-DNP can be used to polarize low-γ nuclei in arbitrary solutions within porous polarizing materials.[20,21] The ^{1}H spins first acquire high polarization under direct DNP in the host material; their high polarization then spreads to the ^{1}H spins in the impregnated solution spontaneously by spin diffusion; the polarization of ^{1}H spins is transferred to the low-γ nuclei in the host solution by CP.[50,51] This process is schematically represented in Figure 4A. After several iterations of CP, the polarization of the low-γ nuclei plateaus. The sample can be dissolved and the polarizing material filtered out.[20] To demonstrate the potential of PANI polymers as polarizing materials for dDNP, ^{13}C spins were hyperpolarized in a host solution impregnated in the pores of a porous PANI polymer by CP-DNP.[20,21] 20 mg of a commercial porous PANI-ES powder were impregnated with 20 µL of a solution of 3 M [1-^{13}C]-sodium acetate in 1:9 H_2O:D_2O (*v*/*v*). The µw frequency was set to 197.630 GHz and modulated at 5 kHz over a bandwidth of 160 MHz at 1.6 K. The polarization was transferred from ^{1}H to ^{13}C spins by µw-gated CP every 4 min as described elsewhere.[50,51] The polarization of the ^{13}C spins during the experiment was monitored every 30 s by a train of four scans with 5° excitation pulses. Fig. 4B shows the ^{13}C signal building up during the multi-CP experiment. Each discontinuity in the curve corresponds to a CP transfer from ^{1}H to ^{13}C spins. Once the ^{13}C signal had plateaued, the temperature of the cryostat was raised to 3.8 K by refilling it with liquid helium at 700 mbar. The decay of the ^{13}C polarization was then monitored at 3.8 K using a train of four scans with 5° excitation pulses every 100 s (see Fig. 4B). The ^{13}C thermal equilibrium signal was not recorded, which prevents the quantification of the polarization during the multi-CP experiment. However, the fact that the signal decays significantly between CP contacts and after the multi-CP experiment at 3.8 K shows that the ^{13}C spins were indeed polarized above thermal equilibrium.

Time Evolution during DNP

Further insights into the intriguing DNP mechanisms in PANI can be obtained by studying the time evolution of ^{1}H polarization under DNP. Figure 5 shows the DNP profile for 28.3 mg of PANI with protonation fraction χ = 0.2, corresponding to an electron spin concentration of 104 ± 7 µmol.mg^{-1}, recorded at 1.6 K as in Fig. 2. The highest absolute polarization is -4.7% and was obtained for an offset frequency of +25 MHz (197.655 GHz in the laboratory frame). Surprisingly, this value is larger than the -2.8% polarization recorded on the same sample (see Fig. 2). The experiments in Fig. 5 were performed on a sample from the same batch as that in Fig. 2 but approx. three weeks later. The aging of the sample seems to have improved its performance. This could be due to absorption of moisture over time as it is known to affect the crystallinity of the polymer and subsequently the mobility of the electrons.[52] The center of the DNP profile features a strong dispersive pattern. On the edges of the spectrum, a slight deviation from the nuclear Boltzmann

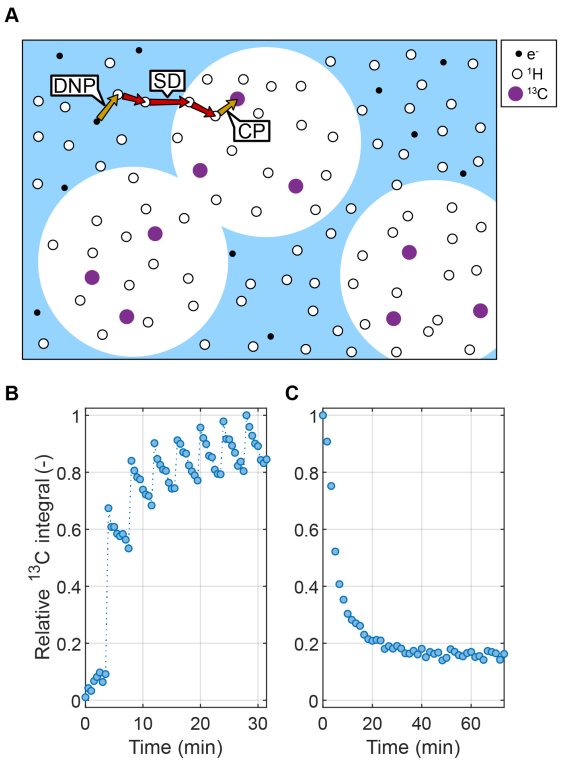

Figure 4: **A**. Schematic representation of CP-DNP in porous polarizing materials, where ^{1}H spins are polarized by direct DNP; ^{1}H polarization spreads from the polarizing material to the impregnated solution by spin diffusion and is then transferred to ^{13}C spins by CP. SD = spin diffusion. **B**. Mutli-CP experiment at 1.6 K in porous ES-PANI impregnated by a solution containing a ^{13}C-labelled analyte, monitored by small-angle pulses. See the text for experimental details. **C**. Decay of the ^{13}C signal at 3.8 K after the build-up of panel B.

polarization is observed at $-\omega_{I0}/2\pi$ = +300 MHz and $+\omega_{I0}/2\pi$ = –300 MHz, where the double- and zero-quantum SE (DQ-SE and SQ-SE) transitions are expected.

The DNP build-up corresponding to each µw frequency was fitted with a stretched exponential function (see Eqs. 2 and 3). The fitted values of T_{av} and β are shown in Fig. 5. The inset above the offset frequency of 25 MHz shows the DNP build-up fitted with Eq. 2 (blue dots and black curve, respectively) for the best performing µw frequency. The model fits the data equally well for all DNP build-ups except for that corresponding to a µw offset frequency of 100 MHz. This DNP build-up has the particularity of going to a positive polarization value on a short time scale before going toward a negative value on a longer time scale (see inset in Fig. 5). This build-up was therefore fitted with a bi-exponential function

$$P(t) = P_{\infty} + (P_{\max} - P_{\infty})e^{-t/T_s} - P_{\max}e^{-t/T_f}, \qquad \text{Eq. 5}$$

where T_s, T_f, P_{∞}, and $P_{\max}$ are the time constants corresponding to the slow and fast processes and the transient polarization toward which the slow and fast processes tend, respectively. The two fitted time constants are shown in black in Fig. 5. The slow and fast time constants appear to be in the continuity of the average time constant coming from the lower and higher µw frequencies,

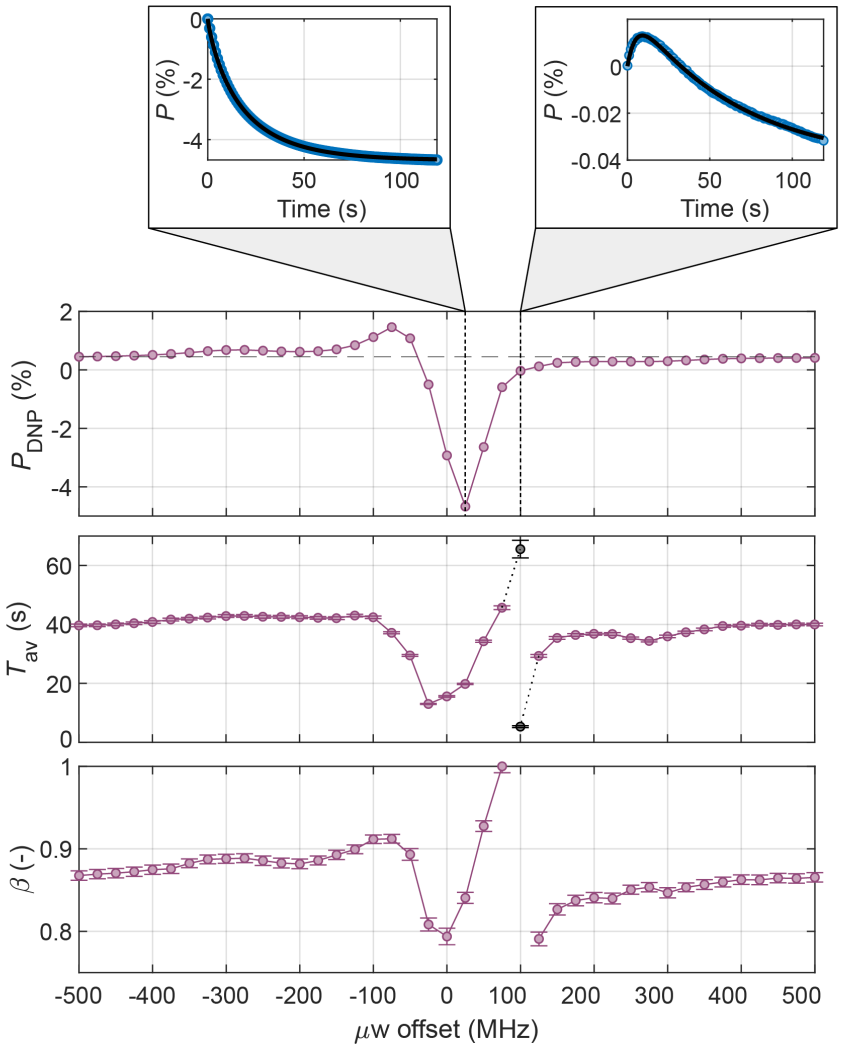

Figure 5: DNP profiles for PANI-EB protonated to level χ = 0.2 (C = 104 ± 7 µmol.mg^{-1}), recorded at 1.6 K and 7.05 T, using 1° pulses. The 0 of µw frequency offset corresponds to a frequency of 197.630 GHz.

respectively, as depicted by the black dashed lines between the data points.

The observation of this anomalous build-up could be explained by two distinct DNP mechanisms acting simultaneously towards positive and negative polarization values, with fast and slow rates, respectively. This explanation is only valid if the two mechanisms act on distinct ^{1}H reservoirs and hence, it must be the result of DNP from distinct electron spin reservoirs. Indeed, two mechanisms acting on a single homogeneous spin reservoir would only result in a single rate constant and hence in a mono-exponential build-up. These two reservoirs could possibly the Pauli and Curie spins, which have different electron mobility and spin-spin interactions. The ^{1}H spin diffusion length in PANI over 10 s is on the order of 25 nm (see the Supplementary Material). This gives an estimate of the minimum separation that the two reservoirs should have for their polarizations to be distinct on the time scale of the DNP build-up. This estimate supports the hypothesis of distinct regions with different radical concentrations and spin properties.

Possible DNP Mechanisms in PANI

As the radical concentration increases, the DNP profiles of Fig. 2 display a crossover from a dispersive pattern to a negative absorptive pattern. These central features can have different origins. As a comparison, Figure 6 shows ^{1}H-DNP profiles for common radicals used for dDNP, namely TEMPOL, trityl, and BDPA in similar conditions. DNP with TEMPOL at a concentration of 50 mM provides the typical conditions for TM/CE-DNP (broad EPR line and strong electron-electron interactions), leading to unresolved positive and negative lobes, with a separation on the order of the nuclear Larmor frequency. Although this feature is most common for DNP at liquid helium temperatures, it is not observed for PANI. The DNP profile of trityl yields expected SE transitions on the edges of the spectrum and a narrow dispersive pattern in the center. Finally, the DNP profile of BDPA yields both SE transitions on the edges and a central positive absorptive pattern in the center.[53] The features observed for trityl and BDPA in Fig. 6 are all found for PANI in Fig. 2.

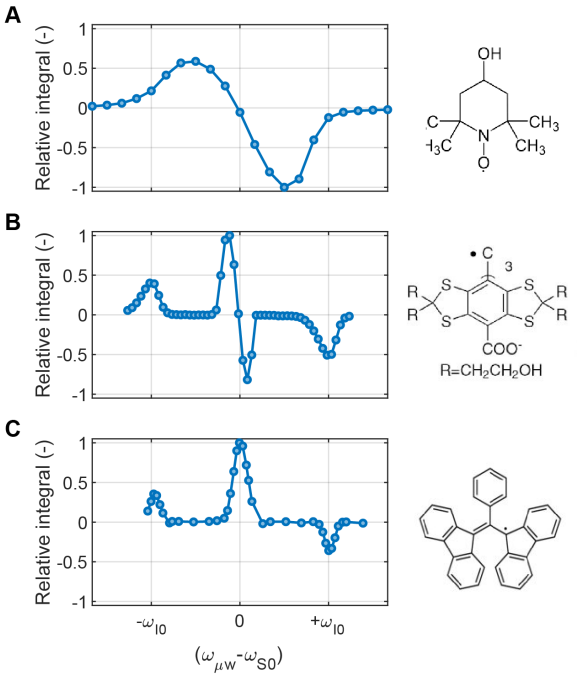

Figure 6: ^{1}H-DNP profiles for 50 mM TEMPOL in DNP juice at 1.6 K and 7.05 T and for 25 mM trityl in neat [1-^{13}C]-pyruvic acid at 1.2 K and 7.05 T (**A** and **B**, respectively) and for polystyrene containing BDPA at 4.2 K and 6.7 T (**C**, Reprinted from Ref. [28], with permission from Elsevier. The values were extracted from the published figure using an online application WebPlotDigitizer). The *x* axis is expressed in units of nuclear Larmor frequency ω_{I0} with respect to the center of the spectrum ω_{S0}.

The dispersive pattern of PANI in Fig. 5 and of trityl in Fig. 6B was observed by other authors in a large range of experimental conditions; Borghini *et al*. observed it using BDPA at 2.5 T and 0.7 K already in 1974,[32] and De Boer explained their results in terms of TM.[54] Karabanov *et al.* later presented full-quantum mechanical simulations of TM in a minimal 3 electron-1 nucleus system[33] that was able to reproduce Borghini *et al*.'s results. The Han group and the Griffin group observed this dispersive pattern using the radicals trityl and BDPA from low to high fields, from 20 to 100 K, and both in static mode and under magic angle spinning (MAS).[34,36,37] Finally, the Prisner group observed a similar pattern for BDPA in lipid bilayers above room temperature.[35] The Han group reported that the effect they observed was stronger at higher radical concentrations.[34] They rationalized this finding based on TM, which would be favored by radical clustering and supported their interpretation using numerical simulations.[34,55] On the other hand, the Griffin group recently proposed a 1 electron-1 nucleus mechanism that they named "resonant mixing" (RM), based on numerical simulations and on an analytical model.[36] The room temperature results of the Prisner group[35] differ from those listed above in that they were acquired in a regime in between liquid and solid dynamics. These results were rationalized by Sezer, who proposed a model of the SE that takes into account the modulation of the hyperfine interaction using Liouville's stochastic equations.[56,57] Both Sezer's model and the Griffin group's RM mechanism rely on the presence of SE transitions (as visible for trityl at $+\omega_{I0}$ and $-\omega_{I0}$ in Fig. 6B). The SE transitions are not visible in the DNP profile where the dispersive feature is most intense (for a radical concentration of 14 ± 7 µmol.mg^{-1}). Therefore, these two mechanisms are unlikely to be at the origin of our observations. To the contrary, the fact that PANI polymers contain both clustered and isolated spins (Pauli and Curie spins, respectively) provides suitable conditions for TM, as proposed by Karabanov *et al*.[33] and the Han group.[34,55]

The absorptive pattern which is negative in Fig. 5 (for high radical concentrations) and positive in Fig. 6C is usually attributed to the OE.[46,53,58] The sign of the enhancement is governed by the imbalance between the DQ and ZQ electron-nuclear cross-relaxation rates and the relative intensity of the dipolar and isotropic electron-nuclear couplings.[59] However, the Han group also suggested that it could be the result of a form of TM in samples where radicals tend to cluster.[55] Their numerical simulations of a 3 electron-1 nucleus spin system showed that subtle changes in the T_{1e} of the different electrons and their respective couplings could lead either to the dispersive pattern of Fig. 6B or the absorptive pattern of Fig. 6C. Both TM and the OE could therefore explain the crossover of the patterns in PANI.

The complex spin properties and morphology of conductive polymers can cause multiple DNP mechanisms to be active at the same time and their relative contribution can be modulated by the electron conductivity.[60] DNP of conductive polyacetylene (PA) at X-band and room temperature was reported in 1980.[12] In this study, a crossover from the SE to the OE was found when PA was converted from *cis* to *trans*, that is, from a form with lower to higher electron mobility.[12,60] As mobility increases, the lifetime of the electron-nuclear hyperfine interactions diminishes, making SE less efficient, while the spectral density of the hyperfine fluctuations at the electron Larmor frequency increases, making the OE more efficient.

In PANI, two explanations could account for the crossover from the dispersive DNP pattern at low radical concentrations to the absorptive pattern at high radical concentrations (see Fig. 2). First, a single mechanism evolves from a dispersive pattern at low radical concentrations into an absorptive pattern at high radical concentrations; second, the DNP profiles are a linear combination of two distinct mechanisms, as for PA.[60] In the first hypothesis, TM with clustered electrons, as simulated by the Han group, could be a possible mechanism, as numerical simulations in a 3 electorn-1 nucleus spin systems showed that variations in T_{1e} and electron-electron couplings could lead to both dispersive and absorptive patterns.[55] The second hypothesis that the crossover is the result of a linear combination of two independent DNP mechanisms is in line with the observation of the anomaly in Fig. 5 where the nuclear polarization changes sign during the DNP build-up. As we have mentioned, TM is the most likely mechanism for the dispersive pattern at low radical concentration while both TM and the OE could explain the absorptive pattern at high concentration. A crossover from TM to the OE with the increase in radical concentration seems likely due to the increase in electron mobility, as was found for PA at X-band and room temperature.[12,60] Indeed, based on reported values of the electron diffusion coefficients $D_{\parallel}$ and $D_{\perp}$ for PANI-EB and PANI-ES down to 4 K,[48,49] we estimate that, as PANI-EB

is converted to PANI-ES, the spectral density of the electron motion at the Larmor frequency of the electron increases by a factor 3, making the OE more efficient (see Eq. S23 and Figure S9). At the same time, the spectral density at 0 frequency decreases by 23%, which implies that electron-electron and electron-nuclear interactions are shorter lived, which is expected to decrease the efficiency of TM or RM.

In summary, we believe that the most probable explanation for the crossover of DNP mechanism with increasing radical concentration (see Fig. 2) is that two distinct mechanisms act simultaneously; at low radical concentration, TM is likely to dominate (and RM would explain the central feature but seems unlikely due to the absence of SE transitions). As radical concentration increases, the probability of the OE increases, while that of all other mechanisms decreases, due to the increase in electron mobility. To further confirm these conclusions, EPR spectra in the same conditions as those of the DNP experiments (i.e., at high field and below 2 K) should be acquired, for example using longitudinally-detected EPR[61] (LOD-EPR) or quasi-optics.[62,63]

Conclusion

We have shown that solid-state ^{1}H-DNP of PANI is possible. Compared to common polarizing agent, PANI polymers polarize faster, albeit to relatively low levels of ≈ 5%. The concentration of electron spins in the polymer was controlled using a simple protocol and was shown to affect the DNP performance and mechanisms. Our data show a complex superposition of DNP mechanisms and provide an interesting basis for their study. We have shown that solid-state DNP using conductive polymers exhibits unusual features compared to insolating samples, due to the complex heterogeneity of the electron mobility and electron spin clustering. Understanding the relation between electron mobility and DNP will probably be important for the optimization of DNP in conductive polymers.

This work represents a first step in the development of dDNP at liquid nitrogen temperatures, without relying on expensive liquid helium. CP-DNP of arbitrary solutions in porous materials where ^{1}H spins are first polarized by direct DNP and ^{13}C spins are subsequently polarized by CP is well established for dDNP at liquid helium temperatures.[20,21] This work brought the proof of principle that CP-DNP in porous PANI is feasible. The next step toward dDNP of arbitrary solutions at N_2 temperatures is the development of porous polarizing materials with chiral properties enabling electron hyperpolarization by CISS.[16] Porous PANI can be synthesized in hydrogels[64], in which the addition of (S)-(2)-2-pyrrolidone-5-carboxylic acid (S-PCA) favors the formation of chiral crystalline structures.[65] The porosity of the porous chiral-PANI can further be controlled by the concentration of the solution during the synthesis, and if required further increased by using a crystallization-induced templating approach.[66] These methods could be used for the preparation of chiral porous conductive polymers as a matrix for efficient nuclear spin hyperpolarization at easily reachable temperatures.

We note that, because the mobility of the electron spins remains active even at very low temperatures, porous PANI polymers might be used to enhance nuclear relaxation for brute-force hyperpolarization at even lower temperatures in the mK range. Indeed, brute force hyperpolarization is often limited by exceeding nuclear relaxation times.[67,68] Paramagnetic nanoparticles have been used to decrease nuclear relaxation times.[68] We envision that low-γ nuclei in solutions impregnated in porous PANI polymers[19] could then be polarized by CP as shown in Fig. 4 after brute-force hyperpolarization of the ^{1}H in the polymer and ^{1}H spin diffusion from the polymer to the solution. The solution could then be extracted from the polymer and used as a dopant-free hyperpolarized solution for liquid-state magnetic resonance.[21]

Supplementary Material

Details about the experimental apparatus, sample preparation, EPR quantification, fitting procedure, and error propagation are available as Supplementary Material.

Data and code availability

The data presented in this work and the MATLAB codes used to analyzed them can be downloaded at the link https://doi.org/10.5281/zenodo.11111533. The processing codes make use of the EasySpin package to open EPR data, and the open-source function rbnmr (available on the MATLAB File exchange portal) to open NMR data.

Conflict of interest

The authors have no conflict of interest to declare.

Acknowledgements

The authors wish to thank Yifan Quan and Joshua Straub for stimulating discussions. This research was supported by ENS-Lyon, the French CNRS, Lyon 1 University, the European Research Council under the European Union's Horizon 2020 research and innovation program (ERC Grant Agreements No. 714519 / HP4all and No. 101044726 / HypFlow, and Marie Skłodowska-Curie Grant Agreement No. 766402 / ZULF) and the French National Research Agency (project HyMag / ANR-18-CE09-0013). The authors gratefully acknowledge Bruker Biospin for providing the prototype dDNP polarizer, and particularly Dmitry Eshchenko, Roberto Melzi, Marc Rossire, Marco Sacher, and James Kempf for scientific and technical support. The authors additionally acknowledge Catherine Jose and Christophe Pages for use of the ISA Prototype Service, and Stéphane Martinez of the UCBL mechanical workshop for machining parts of the experimental apparatus.

References

[1] J. Eills, D. Budker, S. Cavagnero, E. Y. Chekmenev, S. J. Elliott, S. Jannin, A. Lesage, J. Matysik, T.

Meersmann, T. Prisner, J. A. Reimer, H. Yang, I. V. Koptyug, *Chem. Rev.* **2023**, *123*, 1417–1551.
[2] J. H. Ardenkjær-Larsen, B. Fridlund, A. Gram, G. Hansson, L. Hansson, M. H. Lerche, R. Servin, M. Thaning, K. Golman, *Proc. Natl. Acad. Sci. U.S.A.* **2003**, *100*, 10158–10163.
[3] S. Jannin, J.-N. Dumez, P. Giraudeau, D. Kurzbach, *Journal of Magnetic Resonance* **2019**, *305*, 41–50.
[4] Z. J. Wang, M. A. Ohliger, P. E. Z. Larson, J. W. Gordon, R. A. Bok, J. Slater, J. E. Villanueva-Meyer, C. P. Hess, J. Kurhanewicz, D. B. Vigneron, *Radiology* **2019**, *291*, 273–284.
[5] S. J. Elliott, Q. Stern, M. Ceillier, T. El Daraï, S. F. Cousin, O. Cala, S. Jannin, *Progress in Nuclear Magnetic Resonance Spectroscopy* **2021**, *126–127*, 59–100.
[6] F. Gorrini, A. Bifone, *Biosensors* **2023**, *13*, 691.
[7] H. W. Van Kesteren, W. Th. Wenckebach, J. Schmidt, *Phys. Rev. Lett.* **1985**, *55*, 1642–1644.
[8] T. R. Eichhorn, A. J. Parker, F. Josten, C. Müller, J. Scheuer, J. M. Steiner, M. Gierse, J. Handwerker, M. Keim, S. Lucas, M. U. Qureshi, A. Marshall, A. Salhov, Y. Quan, J. Binder, K. D. Jahnke, P. Neumann, S. Knecht, J. W. Blanchard, M. B. Plenio, F. Jelezko, L. Emsley, C. C. Vassiliou, P. Hautle, I. Schwartz, *J. Am. Chem. Soc.* **2022**, *144*, 2511–2519.
[9] A. W. Overhauser, *Phys. Rev.* **1953**, *92*, 411–415.
[10] T. R. Carver, C. P. Slichter, *Phys. Rev.* **1953**, *92*, 212–213.
[11] Z. Miao, F. J. Scott, J. Van Tol, R. Bowers, A. S. Veige, F. Mentink-Vigier, *Soliton Based Dynamic Nuclear Polarization: An Unexpected Overhauser Effect in Cyclic Polyacetylene at High Field and Room Temperature*, Chemistry, **2023**.
[12] M. Nechtschein, F. Devreux, R. L. Greene, T. C. Clarke, G. B. Street, *Phys. Rev. Lett.* **1980**, *44*, 356–359.
[13] K. Ray, S. P. Ananthavel, D. H. Waldeck, R. Naaman, *Science* **1999**, *283*, 814–816.
[14] F. Evers, A. Aharony, N. Bar-Gill, O. Entin-Wohlman, P. Hedegård, O. Hod, P. Jelinek, G. Kamieniarz, M. Lemeshko, K. Michaeli, V. Mujica, R. Naaman, Y. Paltiel, S. Refaely-Abramson, O. Tal, J. Thijssen, M. Thoss, J. M. van Ruitenbeek, L. Venkataraman, D. H. Waldeck, B. Yan, L. Kronik, *Advanced Materials* **2022**, *34*, 2106629.
[15] R. Naaman, D. H. Waldeck, *J. Phys. Chem. Lett.* **2012**, *3*, 2178–2187.
[16] L. Jia, C. Wang, Y. Zhang, L. Yang, Y. Yan, *ACS Nano* **2020**, *14*, 6607–6615.
[17] J. Milani, F. Saenz, C. Roussel, J. Ansermet, *Magnetic Reson in Chemistry* **2022**, mrc.5321.
[18] S. Mishra, A. Kumar, M. Venkatesan, L. Pigani, L. Pasquali, C. Fontanesi, *Small Methods* **2020**, *4*, 2000617.
[19] W. Li, M. Wan, *Synthetic Metals* **1998**.
[20] M. Cavaillès, A. Bornet, X. Jaurand, B. Vuichoud, D. Baudouin, M. Baudin, L. Veyre, G. Bodenhausen, J.-N. Dumez, S. Jannin, C. Copéret, C. Thieuleux, *Angew. Chem.* **2018**, *130*, 7575–7579.
[21] T. El Daraï, S. F. Cousin, Q. Stern, M. Ceillier, J. Kempf, D. Eshchenko, R. Melzi, M. Schnell, L. Gremillard, A. Bornet, J. Milani, B. Vuichoud, O. Cala, D. Montarnal, S. Jannin, *Nat Commun* **2021**, *12*, 1–9.
[22] V. I. Krinichnyi, *Applied Physics Reviews* **2014**, *1*, 021305.
[23] J. M. Ginder, A. F. Richter, A. G. MacDiarmid, A. J. Epstein, *Solid State Communication* **1987**, *63*, 97–101.
[24] K. Mizoguchi, M. Nechtschein, J.-P. Travers, C. Menardo, *Phys. Rev. Lett.* **1989**, *63*, 66–69.
[25] Z. H. Wang, C. Li, E. M. Scherr, A. G. MacDiarmid, A. J. Epstein, *Phys. Rev. Lett.* **1991**, *66*, 1745–1748.
[26] Z. H. Wang, E. M. Scherr, A. G. MacDiarmid, A. J. Epstein, *Phys. Rev. B* **1992**, *45*, 4190–4202.
[27] V. I. Krinichnyi, S. D. Chemerisov, Ya. S. Lebedev, *Phys. Rev. B* **1997**, *55*, 16233–16244.
[28] M. Canales, J. Torras, G. Fabregat, A. Meneguzzi, C. Alemán, *J. Phys. Chem. B* **2014**, *118*, 11552–11562.
[29] M. Lapkowski, E. M. Geniés, *Journal of Electroanalytical Chemistry and Interfacial Electrochemistry* **1990**, *279*, 157–168.
[30] M. Nechtschein, F. Genoud, C. Menardo, K. Mizoguchi, J. P. Travers, B. Villeret, *Synthetic Metals* **1989**, *29*, 211–218.
[31] M. Chipara, G. Aldica, D. Hui, M. Dimonie, K. T. Lau, L. Georgescu, I. Munteanu, H. Marascoiu, *Journal of Optoelectronics and Advanced Materials* **2004**, *6*, 297–30.
[32] M. Borghini, W. De Boer, K. Morimoto, *Physics Letters A* **1974**, *48*, 244–246.
[33] A. Karabanov, G. Kwiatkowski, C. U. Perotto, D. Wiśniewski, J. McMaster, I. Lesanovsky, W. Köckenberger, *Phys. Chem. Chem. Phys.* **2016**, *18*, 30093–30104.
[34] A. Equbal, Y. Li, T. Tabassum, S. Han, *J. Phys. Chem. Lett.* **2020**, *11*, 3718–3723.
[35] A. A. Kuzhelev, D. Dai, V. Denysenkov, T. F. Prisner, *J. Am. Chem. Soc.* **2022**, *144*, 1164–1168.
[36] Y. Quan, Y. Ouyang, M. Mardini, R. S. Palani, D. Banks, J. Kempf, W. T. Wenckebach, R. G. Griffin, *J. Phys. Chem. Lett.* **2023**, *14*, 7007–7013.
[37] C. Tobar, K. Albanese, R. Chaklashiya, A. Equbal, C. Hawker, S. Han, *J. Phys. Chem. Lett.* **2023**, *14*, 11640–11650.
[38] W. Th. Wenckebach, *Journal of Magnetic Resonance* **2019**, *299*, 124–134.
[39] K. Mizoguchi, M. Nechtschein, J. P. Travers, C. Menardo, *Synthetic Metals* **1989**, *29*, 417–424.
[40] S. F. J. Cox, S. F. J. Read, W. T. Wenchebach, *J. Phys. C: Solid State Phys.* **1977**, *10*, 2917–2936.
[41] A. W. Overhauser, *Phys. Rev.* **1953**, *89*, 689–700.
[42] A. Chessari, S. F. Cousin, S. Jannin, Q. Stern, *Phys. Rev. B* **2023**, *107*, 224429.
[43] F. Devreux, J.-P. Boucher, M. Nechtschein, *J. Phys. France* **1974**, *35*, 271–285.
[44] F. Devreux, *Phys. Rev. B* **1976**, *13*, 4651–4657.
[45] K. Mizoguchi, *Japanese journal of applied physics* **1995**, *34*, 1–19.
[46] S. Pylaeva, K. L. Ivanov, M. Baldus, D. Sebastiani, H. Elgabarty, *J. Phys. Chem. Lett.* **2017**, *8*, 2137–2142.
[47] A. Gurinov, B. Sieland, A. Kuzhelev, H. Elgabarty, T. D. Kühne, T. Prisner, J. Paradies, K. L. Ivanov, S. Pylaeva, *Angew. Chem. Int. Ed.* **2021**, *60*, 15371–15375.
[48] F. L. Pratt, S. J. Blundell, W. Hayes, K. Nagamine, K. Ishida, A. P. Monkman, *Phys. Rev. Lett.* **1997**, *79*, 2855–2858.
[49] K. Mizoguchi, K. Kume, *Solid State Communication* **1994**, *89*, 971–975.
[50] A. Bornet, A. Pinon, A. Jhajharia, M. Baudin, X. Ji, L. Emsley, G. Bodenhausen, J. H. Ardenkjaer-Larsen, S. Jannin, *Phys. Chem. Chem. Phys.* **2016**, *18*, 30530–30535.
[51] S. J. Elliott, M. Ceillier, O. Cala, Q. Stern, S. F. Cousin, S. Jannin, *Journal of Magnetic Resonance Open* **2022**, *10–11*, 1–12.
[52] P. K. Kahol, A. J. Dyakonov, B. J. McCormick, *Synthetic Metals* **1997**, *89*, 17–28.
[53] X. Ji, T. V. Can, F. Mentink-Vigier, A. Bornet, J. Milani, B. Vuichoud, M. A. Caporini, R. G. Griffin, S. Jannin,

M. Goldman, G. Bodenhausen, *Journal of Magnetic Resonance* **2018**, *286*, 138–142.
[54] W. De Boer, *J Low Temp Phys* **1976**, *22*, 185–212.
[55] Y. Li, A. Equbal, T. Tabassum, S. Han, *J. Phys. Chem. Lett.* **2020**, *11*, 9195–9202.
[56] D. Sezer, *Magn. Reson.* **2023**, *4*, 129–152.
[57] D. Sezer, *Magn. Reson.* **2023**, *4*, 153–174.
[58] T. V. Can, M. A. Caporini, F. Mentink-Vigier, B. Corzilius, J. J. Walish, M. Rosay, W. E. Maas, M. Baldus, S. Vega, T. M. Swager, R. G. Griffin, *The Journal of Chemical Physics* **2014**, *141*, 064202.
[59] L. Delage-Laurin, R. S. Palani, N. Golota, M. Mardini, Y. Ouyang, K. O. Tan, T. M. Swager, R. G. Griffin, *J. Am. Chem. Soc.* **2021**, *143*, 20281–20290.
[60] B. H. Robinson, A. R. Coffino, *Phys. Rev. Lett.* **1990**, *64*, 1773–1776.
[61] J. Granwehr, J. Leggett, W. Köckenberger, *Journal of Magnetic Resonance* **2007**, *187*, 266–276.
[62] P. Neugebauer, A.-L. Barra, *Appl Magn Reson* **2010**, *37*, 833–843.
[63] T. A. Siaw, A. Leavesley, A. Lund, I. Kaminker, S. Han, *Journal of Magnetic Resonance* **2016**, *264*, 131–153.
[64] H. Guo, W. He, Y. Lu, X. Zhang, *Carbon* **2015**, *92*, 133–141.
[65] Y. Yang, M. Wan, *J. Mater. Chem.* **2002**, *12*, 897–901.
[66] D. Khedaioui, C. Boisson, F. D'Agosto, D. Montarnal, *Angew Chem Int Ed* **2019**, *58*, 15883–15889.
[67] M. L. Hirsch, N. Kalechofsky, A. Belzer, M. Rosay, J. G. Kempf, *J. Am. Chem. Soc.* **2015**, *137*, 8428–8434.
[68] J. R. Owers-Bradley, A. J. Horsewill, D. T. Peat, K. S. K. Goh, D. G. Gadian, *Phys. Chem. Chem. Phys.* **2013**, *15*, 10413.